EXPERIMENTAL AND COMPUTATIONAL STUDY OF RIBBED CLADDING FOR PWR ROD BUNDLES HEAT TRANSFER ENHANCEMENT

L. A. Carrilho[*], M. B. Dzodzo[+]
Westinghouse Electric Company
[*]5801 Bluff Road, Hopkins, SC 29061, USA
[+]1000 Westinghouse Drive, Cranberry, PA 16066, USA
carrilla@westinghouse.com; dzodzomb@westinghouse.com

J. A. Khan
Department of Nuclear Engineering
University of South Carolina
300 Main Street, Columbia, SC 29208, USA
khan@cec.sc.edu

ABSTRACT

PWRs fuel assemblies utilize spacer grids with flow mixing vanes to generate lateral flows and augment the coolant turbulence intensity and improve convective heat transfer from the fuel rods surface. However, the large eddy structures and turbulence intensity generated due to mixing vanes decays downstream of the spacer grids so the benefit is reduced as a function of distance. Artificial roughness will improve convective heat transfer at fuel rod surface as it acts as a boundary layer disturbance in the near-wall turbulent flow to promote higher momentum and more uniform heat transport along the surface of the rod. The empirical correlations based on the gas cooled fuel rod rough surfaces test data were used by Meyer et al [15] to perform an analysis to predict heat transfer and friction factor increases for artificially roughened fuel rod bundles at High Performance Light Water Reactors, but their applicability has never been experimentally confirmed. A Single Heater Element Loop Tester (SHELT) was designed to investigate the use of the artificial roughness for improved heat transfer in PWR rod bundles. The observations during the experiments included measurements of volumetric flow rate, electrical power, differential pressure, water and heated single rod wall temperatures across the smooth and the ribbed surfaces at pressures and temperatures in the range of 0.2 to 0.5 MPa and 20 to 120°C, respectively. Also, the corresponding Computational Fluid Dynamics (CFD) model of conjugated heat transfer was developed and validated by comparing with experimental results. This study shows that transverse square ribs improve heat transfer in PWR rod bundles by a factor of 1.47. On the other hand, the friction factor results indicate an increase in flow resistance by a factor of 1.50. Further studies are needed to check if an application of helical ribs might reduce the flow resistance without significant decrease of the obtained heat transfer enhancement.

KEYWORDS
Nuclear fuel rod, artificial roughness, test loop, convective heat transfer, CFD

1. INTRODUCTION

Modern PWR fuel assembly designs rely on mixing vanes for improved heat transfer within fuel rod bundles. These vanes generate global flow turbulence in the form of lateral flows and swirls, which

disturb the boundary layers near the surface of the fuel rods, resulting in heat transfer enhancement. In a more generalized form, the energy of the axial flow at the mixing vanes is transformed into global turbulence energy, which generates local resistance to the flow. Next, energy losses are incurred, e.g. by vortexes that gradually dissipate downstream of the vanes and impact the rod bundle. This behavior provides the desired disturbance of the boundary layer at the rod bundle surface. However, after an appropriate development length, the time-averaged axial velocity exhibits a constant or very nearly constant span wise profile [1, 2]. In addition, the time-averaged mass flow rate through each individual sub channel does not change with increasing axial distance [1]. This indicates that the inlet conditions or support grids no longer affect the global flow distribution through the rod bundle. Since this global flow turbulence is very irregular and rapidly dissipates downstream from the vanes, the heat transfer coefficient is the lowest close to the end of the span between the grids, resulting in limiting conditions.

One of the earliest and perhaps simplest and yet highly effective techniques for improving heat transfer in heated flow channels is the use of surface roughness in turbulent flows. It essentially disturbs the viscous sub layer in the near-wall turbulent flow structure to promote higher momentum and heat transport. Much of the early work, from [3], focused on "naturally" occurring roughness in commercial tubes. However, because such natural roughness is not well defined, artificial or structured roughness is now commonly employed in most applications. Structured roughness can be integral to the surface by machining (e.g., knurling, threading, grooving), forming casting, or welding, and the resulting surface protuberances or grooves can be two-dimensional or discrete three-dimensional in their geometrical arrangement. As a result, an infinite number of geometric variations are possible for structured roughness, and this is also reflected in extensive studies. Since the equivalent sand roughness concept as in [3] does not really represent a structured roughness whose parameters, e.g. height, width, pitch, needs to be accounted in a design optimization, the effects of artificially roughened tubes on heat transfer and pressure drop in turbulent flow of water has been studied by investigators of whom the most related to the present study is briefly mentioned here. Also, a review of the relevant research that addresses the heat transfer enhancement in nuclear fuel rod bundles obtained with the roughening technique is summarized next.

Dippery and Sabersky [4] developed correlations for water flow friction and heat transfer in smooth and rough pipes at various Reynolds and Prandtl numbers. The resulting expressions for friction factor and velocity distribution are essentially the same as those previously developed by Nikuradse.

Tong et al [5] tested a single tube artificially roughened with transverse circular ribs to evaluate the effect of the ribbed rod surface on Critical Heat Flux (CHF) in the sub cooled water flow at typical PWR operating conditions. The sub cooled CHF remained unaltered at the ribbed rod surface with circular ribs of 63.5 μm height. So, the conclusion was that if the rib is not sufficiently greater than the thickness of the superheated liquid layer, the near-wall flow pattern should not be altered.

Donne and Meyer [6] reported heat transfer and friction coefficients from experiments at ribbed surfaces with two-dimensional rectangular ribs for the purpose of improved heat transfer in gas-cooled reactor cores. Their research illustrates a transformation method to obtain data applicable to reactor fuel arrays from annulus experiments. The experiment was performed on an annular test section with gas and a concentric single ribbed heater rod. The experimental data were adjusted for rod array boundary conditions analyzed using a transformation method based on the universal laws of the wall. The main results are: a new transformation method for friction and heat transfer coefficients has been developed; the applicability of the Nikuradse universal velocity profile has been confirmed; and correlations have been determined for heat transfer experimental data. The authors also presented data from open literature adjusted with the proposed method and the resulting correlations for fully rough flow.

Gee and Webb [7] reported heat transfer and friction factor results obtained from ribbed surfaces with helical ribs in heat exchangers. The experimental program consisted of measuring heat transfer and

friction characteristics of the helical rib surface geometry inside a circular tube with air flow for three different helix angles. The data correlation was performed using Nikuradse's equation [3] for the friction and Dippery & Sabersky's [4] for the heat transfer. The analysis shows higher heat transfer for the helical rib than for the transverse rib roughness. Among the three proposed helix angles, the 49 degrees showed the best performance.

Meyer [8-10] considered two different three-dimensional roughness elements for the purpose of heat transfer enhancement in gas-cooled reactors. The tests were performed in an annular large scale test section with air and a concentric single rough heater rod. The heat transfer and pressure loss measurements at single rods with different three-dimensional roughness in different flow housings were reported. The three-dimensional roughness test results showed considerably higher heat transfer than the two-dimensional roughness.

Firth [11] reanalyzed the heat transfer test data obtained by Meyer [8, 9] by using the eddy diffusivity transformation method and concluded that the methods developed for two-dimensional roughness cause a significant discrepancy of the results when used to analyze experimental data obtained from three-dimensional roughness. This could be associated with the substantial increase in eddy diffusivity caused by the three-dimensional roughness. The three-dimensional diamond shape roughness results showed a thermal performance 20% higher when compared with all the other surfaces considered. However, the data is too limited to determine the optimum three-dimensional roughness design.

Firth and Meyer [12] compared four different types of artificially roughened surface in terms of heat transfer and friction factor performance with the purpose of improving heat transfer rates within gas-cooled reactor fuel bundles. The tests were performed in turbulent annulus gas flows with electrically heated single roughened tubes inside no heated smooth outer tubes. The three-dimensional roughness showed an improvement of approximately 8 to 15% compared to the two-dimensional ribbed surfaces.

Ravigururajan and Bergles [13] developed and verified general correlations for friction factor and heat transfer coefficient for single phase turbulent flow in internally roughened tubes. They gathered a wide range of tube and flow parameters previously investigated for different roughness geometries, including transverse square ribs. Experimental tests confirm the applicability of the correlations for a wide range of roughness types. According to the results, the correlations show to be an improvement to those presented by others investigators, for the selected range of parameters.

Dimitrakopoulos [14] developed a new method to predict displacements of fluid droplets from solid surfaces during coating processes. The method is based on a previous work, which employs the spectral boundary element method to determine the equilibrium shape of fluid droplets attached to a solid surface in a viscous shear flow. Several equilibrium shapes were determined for droplets under different viscosity conditions. The method can be used to indicate an element shape for distributed roughness minimum friction loss.

Meyer et al [15] proposed a fuel cladding design with two-dimensional roughness in order to improve heat transfer in fuel assemblies for High Performance supercritical Light Water Reactors. His roughness design is based on previous investigations for gas-cooled reactors [8-10] and the transformation method developed by Gee and Webb [7]. The heat transfer increase for a fuel assembly taking into account the vertical and the cross mass flows is in the order of a factor of two compared with smooth claddings.

It might be concluded that substantial studies for applicability of artificial roughness were performed mainly for gas cooled reactors applications. Effects of artificial roughness for light water reactors were also studied, however, except for Tong et al [5], no testing was performed to confirm or to correct the results.

Therefore, the purpose of this research is to experimentally quantify the convective heat transfer and the accompanied flow resistance obtained with a selected artificial roughness design by testing a single simulated fuel rod in water turbulent flow. The experimental investigation is accomplished by measuring the single phase water temperatures, surface temperatures, and the differential pressures between the smooth and the ribbed surface sections of a single heated tube inside of concentric smooth and unheated circular flow housing. The choice of a two-dimensional roughness with transverse square shape for this investigation is dictated by the geometrical simplicity and the extensive prior studies involving similar roughness design. The test facility is designed to simulate PWR operating conditions based on the similarity concept.

The experimental work is further enhanced with a numerical model, using the Computational Fluid Dynamics (CFD) and the conjugate heat transfer analysis based on the Finite Element Method (FEM). The CFD model is benchmarked and used to analyze the flow field and the convective heat transfer on the ribbed surface of the tested simulated fuel rod so that it can be used to investigate further modifications of the roughness design for improved heat transfer and differential pressure performance.

2. EXPERIMENTAL TESTING

2.1. Test Section

The experimental heat transfer study relies on the Single Heater Element Loop Tester (SHELT) thermal hydraulics loop constructed at the University of South Carolina (USC). A schematic of the SHELT loop is presented in Fig. 1. The major features of the loop include: test section, loop, electrical system, instrumentation, and data acquisition system.
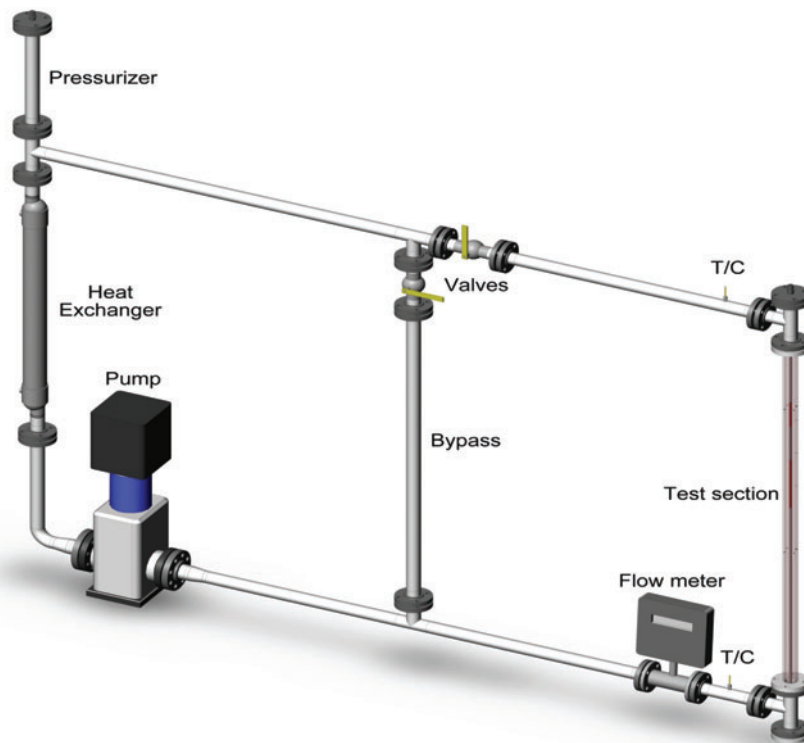
Figure 1. SHELT Loop.

The SHELT loop piping is constructed from 304 stainless steel, schedule 40s piping, including ball valves, elbows, and tees. The loop is attached to a board parallel to the wall. There are several advantages from this configuration, e.g. flow stability and reduced vibration of the system as all components are coplanar between them. The pump is a vertical inline multi-stage booster pump with all wetted parts constructed from 304 series stainless steel, with a flow capacity of 15 m³/h against a 10 m head. When the heated water exits the test section, it flows through the loop piping and then through a single-pass heat exchanger constructed from 316 stainless steel for cooling to the desired inlet temperature. A column of air, pressurized by an air compressor, sets the system pressure. The pressurizer is constructed from 304 stainless steel piping partially filled with water above the loop. The SHELT loop bypass and test section valves control the water flow rate in the loop. One is located at the exit of the bypass and the other at the exit of the test section. A precision valve made of brass controls the water flow rate at the exit of the heat exchanger. The power supply consists of two units connected in series in order to provide 20 volts, 500 amperes and 10 kW power. The measurements performed during the pressure drop and the heat transfer experiments, and the instrumentation needed to operate the SHELT loop, include: test section inlet flow rate; water temperature at the inlet and outlet of the test section; total pressure of the system; differential pressures between axial points in the test section; total DC power to the test section; temperatures at different axial points of the heater rod wall. The loop includes three turbine flow meters, two to measure the total flow rate through the test section at lower and higher flow ranges, and the third to measure the flow rate of the cooling water through the heat exchanger. Two thermocouples are used to measure the inlet and the outlet temperatures. A gauge pressure transmitter connected at the bottom of the test section provides the total system pressure readings.

Major requirements for the aluminum tube annular test section design include: 10 bar maximum pressure, 200°C maximum temperature, and 50 mm insulation in order to reduce heat loss and improve energy balance. The annular cross sectional geometry simulates a typical rod bundle sub channel, i.e. the rod diameter of 9.5 mm is converted to a single rod annulus based on the hydraulic diameter concept:

$$D_h = 4A_f / P_w$$

For flow geometry around a center rod in typical rod bundle (Fig. 2a), the wet perimeter is calculated, as follows:

$$P_w = 4\pi\, d_o/4 + 4\pi\, d_o/4 + 8p_r - 8d_o$$

Hence, the housing inner diameter is calculated as

$$d_{eq} = P_w/\pi$$

for an equivalent circular sub channel, as shown in Fig. 2b.

To straighten the flow before it reaches the test section, the heater rod is designed to have a minimum of twenty hydraulic diameters length upstream the heater rod test section down to the inlet tee. The housing also includes two sets of ceramic rod supports ten hydraulic diameters upstream and downstream of the test section to assure alignment of the test rod with the centerline of the annulus outer tube (Fig. 3a). The rod assembly is connected to the test section by press fitting the lower end with two ring seals against the bottom flange, which provides a free expanding end, as such accommodating an eventual thermal expansion of the heater rod. The upper end is connected by means of a tube fitting screwed in the top flange.
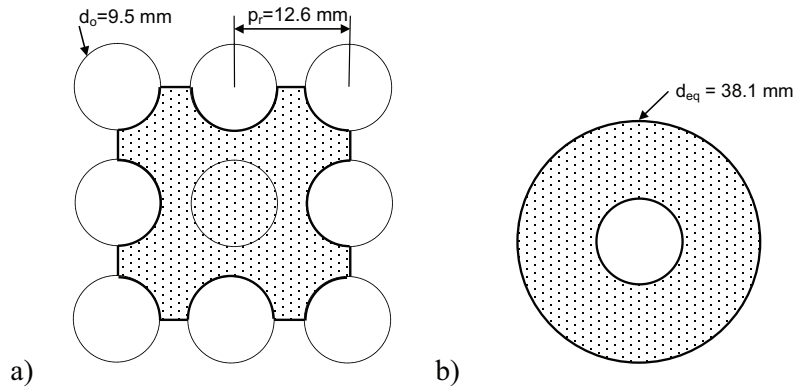
Figure 2. a) Typical Rod Bundle Sub-Channel, b) Equivalent Circular Annulus Sub-Channel

Bushings between bolts and flange electrically insulate the flow housing from the electrically heated rod. The heater rod assembly consists of three concentric rod and tubes assembled in line, designed to generate most the heat in the higher resistivity Inconel 625 test section. A lower resistivity nickel 200 rod is brazed to the Inconel tube, which is brazed to a nickel 200 tube to simulate a desirable axial power distribution. The rod assembly also includes a movable thermocouple probe (Fig. 3b) inserted during the brazing process. The probe is designed to rotate and slide up and down from a thin rod, passing through the nickel tube. Fig. 4 c shows the thermocouple stop locations at the test section for the temperature measurements.

Fig. 3d shows the ribbed surface details of the single rod. In this section, a multiplicity of square ribs is evenly distributed over the rod length, starting at 234 mm downstream the beginning of the Inconel heater tube. The rib parameters are: 0.127 mm height, h, and width; $9h$ pitch of ribs; 9.5 mm heater tube outer diameter; 38.1 mm housing inner diameter.

Three differential pressure transmitters in series provide the measurements of flow resistance across the smooth and the ribbed surfaces of the simulated fuel rod. The first pressure transmitter measures the differential pressure across the smooth surface of the rod, the second transmitter measures the differential pressure associated with the ribbed surface, and the third transmitter measures the total flow resistance across both smooth and ribbed surfaces for a total pressure difference check. The pressure tap locations relative to the smooth and ribbed span locations are shown in Fig. 3e.

The primary controlled parameter in the hydraulic testing is the annulus flow rate. The maximum flow rate is achieved in increments of 2 m³/h. At maximum conditions, the SHELT loop can achieve Reynolds and Prandtl numbers typical at PWRs. The loop provides a minimum temperature difference of 10°C between the rod and the coolant, which is expected to be reasonable for accuracy of the heat transfer results. The test parameters, including system pressure, water flow rate, inlet temperature, and estimated test section power, consists of a nominal number of four heat transfer points for the test. The nominal range of parameters is: 0.2 - 0.5 MPa system pressure; 0.2 - 2.0 kPa differential pressure; 0.1 - 14 m³/h water flow rate; 0 - 10 kW power; 20 - 120°C water temperature; 20 - 140°C rod temperature. These conditions are supposed to provide satisfactory thermal hydraulic conditions that are typically similar to PWR's. The data acquisition system used in conjunction with the SHELT loop is comprised of a digital computer system, analyzers and several analog conversion subsystems. Monitor and displays provide real time observance of the flow rate, pressure, and temperature parameters.
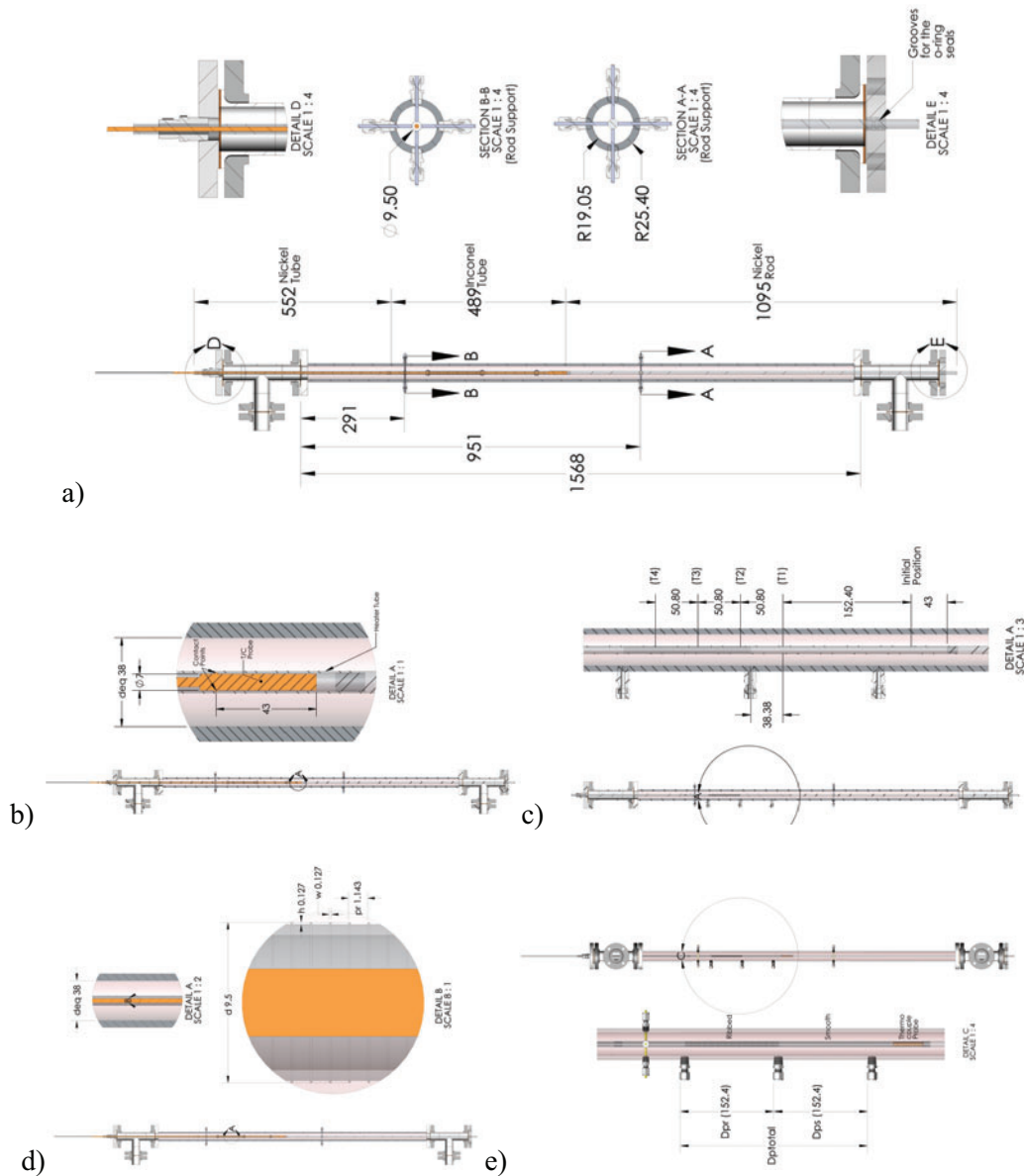
Figure 3. a)Test Section; b) Thermocouple Probe; c) Thermocouple Stop Locations; d) Ribbed Section and Roughness Parameters; e) Pressure Tap Locations. (dimensions are in millimeters)

2.2. Test Plan

The equations presented in this section are used to convert the differential pressure values to friction factors and the temperatures to heat transfer coefficients for different flow conditions. The calculations are based on the flow area and equivalent diameter of the single heater rod inside the flow housing. The pressure drop and the temperature are measured at locations such that friction factors and heat transfer coefficients can be obtained for smooth and ribbed surfaces of the rod. The flow area and the hydraulic diameter parameters are calculated for concentric outer and inner circular tubes (annulus) of the test section. At the beginning of the experimental program, prior to the heat transfer tests, ten differential pressure readings are taken for a selected range of flow rates at room temperature. The nominal loop

conditions for the pressure drop test were 0.3 MPa and 20°C, respectively. The selected seven flow rates sequentially run in the pressure drop test varied from 6 to 12 m³/h with increments of 1 m³/h. The next step involves reducing the test data by averaging differential pressure results over each of the ten data sets and calculating the corresponding friction factors, as follows:

$$f = \left(4W^2 - \pi d_o^2\right)^3 \Delta_P \Big/ 32\left(4W + \pi d_o\right)Q^2 \rho l$$

The resulting friction factor values are compared to the correlation proposed by Haaland [16]:

$$f^{-1/2} = -1.8\log_{10}\left[6.9\big/\mathrm{Re} + \left(k_s\big/D_h\big/3.7\right)^{1.11}\right]$$

After the pressure drop test, before the heat transfer test, the lab team conducted a heat balance test to confirm the accuracy of the loop instrumentation and to determine heat losses. The tests were performed after the test loop had reached steady state conditions for the parameters: 0.5 MPa system pressure; 0.23 m³/h flow rate; 38°C inlet temperature; 3.2 kW power. The team used the following equation to calculate the heat losses:

$$\text{Heat Loss \%} = \left[1 - \left(H_{out} - H_{in}\right)\big/q\big/\dot{m}\right]\times100$$

The convective heat transfer coefficient is defined by the relationship,

$$U = q\big/A_s\left(T_w - T_b\right)$$

The bulk fluid temperature at a given axial location is determined from a linear interpolation between inlet and outlet mean temperatures. This analysis uses the below conduction equation to calculate the temperature on the outer surface of the simulated fuel rod:

$$T_w = T_{w,i} - \dot{q}\left(2d_i^2 \ln d_i\big/d_o - d_i^2 + d_o^2\right)\big/16k$$

The thermocouple probe readings of temperature obtained at the inner surface of the heater tube and the temperature calculated at the outer surface, using the above conduction equation, are used in the calculation of the heat transfer coefficient. The heat generation rate is calculated, as follows:

$$\dot{q} = 4q\big/\pi\left(d_o^2 - d_i^2\right)l$$

For the ribbed surface heat transfer and friction loss, this research relies on correlations and numerical calculations, as there is no analytical solution for temperatures on this type of uneven surface. Assuming radiation and conductive heat transfer losses to be negligible, the energy balance yields "power in = rate of energy transferred by convection" or

$$q = EI = U\left(\pi d_o l\right)\left(T_w - T_b\right)$$

Therefore, solving for the experimental results,

$$U = q_{inc}\big/\pi d_o l\left(T_w - T_b\right)$$

The total power dissipated in the simulated fuel rod is determined based on the current and the voltage measurements or electrical resistance:

$$q = IE = I^2 R$$

The heat dissipated by the Inconel portion of the test rod, qinc, is determined based on the heat dissipated within the test section and the heat dissipated by the nickel portion of the rod located within the test section upstream (nickel rod) and downstream (nickel tube) of the Inconel tube:

$$q_{inc} = q - I^2 R_{NiRod} - I^2 R_{NiTube}$$

with

$$R = \rho_e l / A$$

The heat transfer coefficient values calculated for the smooth section of the simulated fuel rod are compared to those obtained from the correlation proposed by Gnielinski [17] for consistency check:

$$Nu = (f/2)(\text{Re} - 10^3)\text{Pr}/1 + 12.7(f/2)^{1/2}\left(\text{Pr}^{2/3} - 1\right)$$

where the friction factor parameter is calculated using the correlation by Haaland [16]. The heat transfer points of temperature are taken after the inlet temperature, the flow rate, and the system pressure are held constant. The current is increased in increments of 20%, with a minimum dwell time of 60 seconds for some stabilization of the water temperature, until it reaches the inlet temperature target. Next, there is a dwell time of two hours for the test loop to reach steady state. As soon as the test loop reaches the steady state conditions, the team takes ten surface temperature readings at specific elevations of the Inconel heater tube, including those of the flowing water at the inlet and the outlet positions of the test section.

The SHELT loop is assumed to be at steady state conditions when the difference between the heated Inconel tube temperatures measured at the beginning and at the end of the acquisition data process is less than 0.5°C. The nominal test conditions for the heat transfer test are: 0.4 MPa system pressure; 5-14 m³/h water flow rate; 100°C inlet temperature; 6 kW power. A bypass line controls the loop flow rate. The bypass valve is set to give the required flow, which is displayed by the flow rate analyzer on top of the flow meter. The annulus velocity is determined from the total loop flow rate and the test section (annulus) flow area. The simulated fuel rod installed in the test section is the major source of heat in the system. In order to control the heat input and keep the inlet temperature in the preferred testing range, the lab team rely on a precision valve that controls the flowing tap water at room temperature through the heat exchanger. The single rod within the flow housing is heated, using resistance heating, in order to measure the convective heat transfer over a fully heated span with smooth and rough surfaces. The nickel rod and tubing have low electrical resistivity (13μΩ-cm at 100°C) and are used to conduct electricity to the Inconel tubing that has a much larger electrical resistivity (133μΩ-cm at 150°C). The power is dissipated through the Inconel tube as heat and provides essentially constant surface heat flux conditions. The rod assembly in the flow housing is connected to the power supply. Electrical connections to the tube are made outside of the test section using custom designed copper connection plates attached to the nickel rods. The voltage drops across the copper connection plates located at the inlet and outlet of the test section and the current through the tube are determined based on the readout of the clamp meter. The heat dissipated in the tube is calculated based on the current and voltage measurements obtained for each test condition. The energy lost by conduction through the test section and radiation from the test section is estimated based on the total heat dissipated in the test section and the heat transferred to the fluid (heat balance check).

3. CFD ANALYSIS

The numerical model is based on a previous CFD analysis developed by Carrilho [18]. The intent with the numerical simulation is to reproduce the mechanisms responsible for the enhanced heat transfer on the ribbed surface. The specific objectives are: 1) calculate the turbulent flow and the differential pressure across the smooth and the ribbed surfaces of the heated tube; 2) calculate the temperature distribution in the flow and the solid domains across the smooth and the ribbed surfaces of the heated tube; 3) compare the CFD analysis results with the experimental data. The analysis procedure combines the CFD and the conjugate heat transfer methods to calculate the temperature distribution in the flow/solid model. The calculation domain consists of an axisymmetric heated tube wall with smooth and ribbed surfaces in turbulent flowing water inside of a smooth unheated circular tube. The CFD analysis uses the FEM to solve the Navier-Stokes and the energy equations in a two-dimensional, axisymmetric, annular, single phase, turbulent flow domain. Since this analysis also seeks to predict the flow pattern in the turbulent boundary layer around the roughness ribs, the CFD technique uses the Shear Stress Transport (SST) turbulence model to solve the flow and the pressure equations in the annular flow domain, including the boundary layer. The SST model divides the flow domain in two regions, combining the k-ω and the standard k-ε models. As contrasted with wall functions, the k-ω model provides a better modeling of the boundary layer as it solves the flow and the pressure equations in this region. The SST model combines the advantages of both models and automatically switches to the k-ω model in the near region and the standard k-ε model away from the walls [19, 20]. The challenge due to the above procedure is that, the required mesh is much denser than the typical wall function based turbulence models. This requirement significantly increases the computation effort. Hence, this analysis uses a dense and structured mesh for near wall regions, providing more consistent representation at the wall with ribs. The mesh criterion establishes that, the first node shall be no farther than y^+=3 from the wall so as to not compromise the flow and the pressure calculation results [20]. The analysis uses the below equation to calculate the friction factors associated with the average pressure drop predicted by CFD across the smooth and the ribbed sections.

$$f = \Delta p (D_h / l) 2 \big/ \rho V_{avg}^2$$

The heat transfer analysis compares the smooth and the ribbed surfaces based on temperatures calculated by the CFD model. Next, it calculates the heat transfer coefficient U based on the power rate q directly obtained from the test results, according to the following equation:

$$U = q \big/ A_s (T_w - T_b)$$

The CFD model consists of a heated rod tube in turbulent flowing water with smooth and ribbed surfaces inside of a smooth unheated circular tube. The model takes advantage of the two-dimensional axisymmetric characteristic of the flow domain to reduce the computing effort. Fig. 4a shows a schematic of the annular geometry.

The geometric parameters used in this analysis are listed in Table 1. It should be noted that, the outer tube material is not modeled as its participation in the heat transfer analysis is considered to be negligible. The meshing strategy involves three main points: two-region domain, element shapes, and meshing gradient. The model uses structured mesh in the smooth region and unstructured mesh in the ribbed region for minimum reasonable number of elements. The ribbed flow radial lines are divided by 100 element size, with a ratio (gradient) of 104, and the flow domain is free meshed with triangle elements. The mesh gradient value corresponds to the ratio between the largest and the smallest element size. The meshing parameters used in this analysis are listed in Table 2.

Table 1. CFD model geometrical parameters

Parameter	Value (mm)	Notes
Rib height, h	0.127	
Pitch of ribs, p	1.143	$9h$
Tube OD, d_o	9.5	
Tube ID, d_i	8.0	
Housing ID, d_{eq}	30.8	Pressure drop analysis
	38.1	Heat transfer analysis
Housing thickness	20	
Hydraulic diameter, D_h	21.3	
Entrance length	852	$40D_h$
Ribbed length	22.86	$(20)(9)h$

Table 2. Meshing parameters

Parameter	Divisions	Size (mm)	Ratio
Near region	20	0.006	1
Rib span	65	0.006 - 0.03	5
Main Flow	100	0.006 - 1.0	104
Entrance	800	0.1 - 5.0	100

Fig. 4b shows the view of the applied mesh and Fig. 4c the element shape distributions at one rib. Note that, the CFD model assumes an entrance length of forty times the hydraulic diameter of the annulus for a fully developed flow.

Since this analysis aims to simulate the heat transfer test performed in the SHELT loop, the thermal properties of the fluid and the Inconel heater tube are based on the test parameters. They are listed in Table 3 for the lowest test conditions. This assumption helps the convergence of the CFD results and delivers a minimum feasible improvement in heat transfer. The boundary and the loading conditions are based on the test parameters selected to evaluate the structured roughness design. The flow domain is defined by the smooth and the ribbed surface of the inner heater rod, and the inner surface of the outer unheated tube. At these surfaces, the fluid velocities are zero. Since the unheated outer tube is not included in the model, setting the velocities to zero at the outer boundary of the flow domain simulates the related wall effect.

For the heat transfer analysis, the outer boundary is assumed to be adiabatic and, therefore, no parameters are specified. The analysis assumes a uniform inlet velocity and temperature. At the outlet, nothing but zero pressure is specified. Finally, a heat generation rate load is applied in the solid domain, representing the test rod heated by electric current. Fig. 4b shows the boundary conditions and the heat generation rate locations of the numerical model.

The flow conditions for the CFD pressure drop and thermal analysis are listed in Table 4.

a)

b)

c)
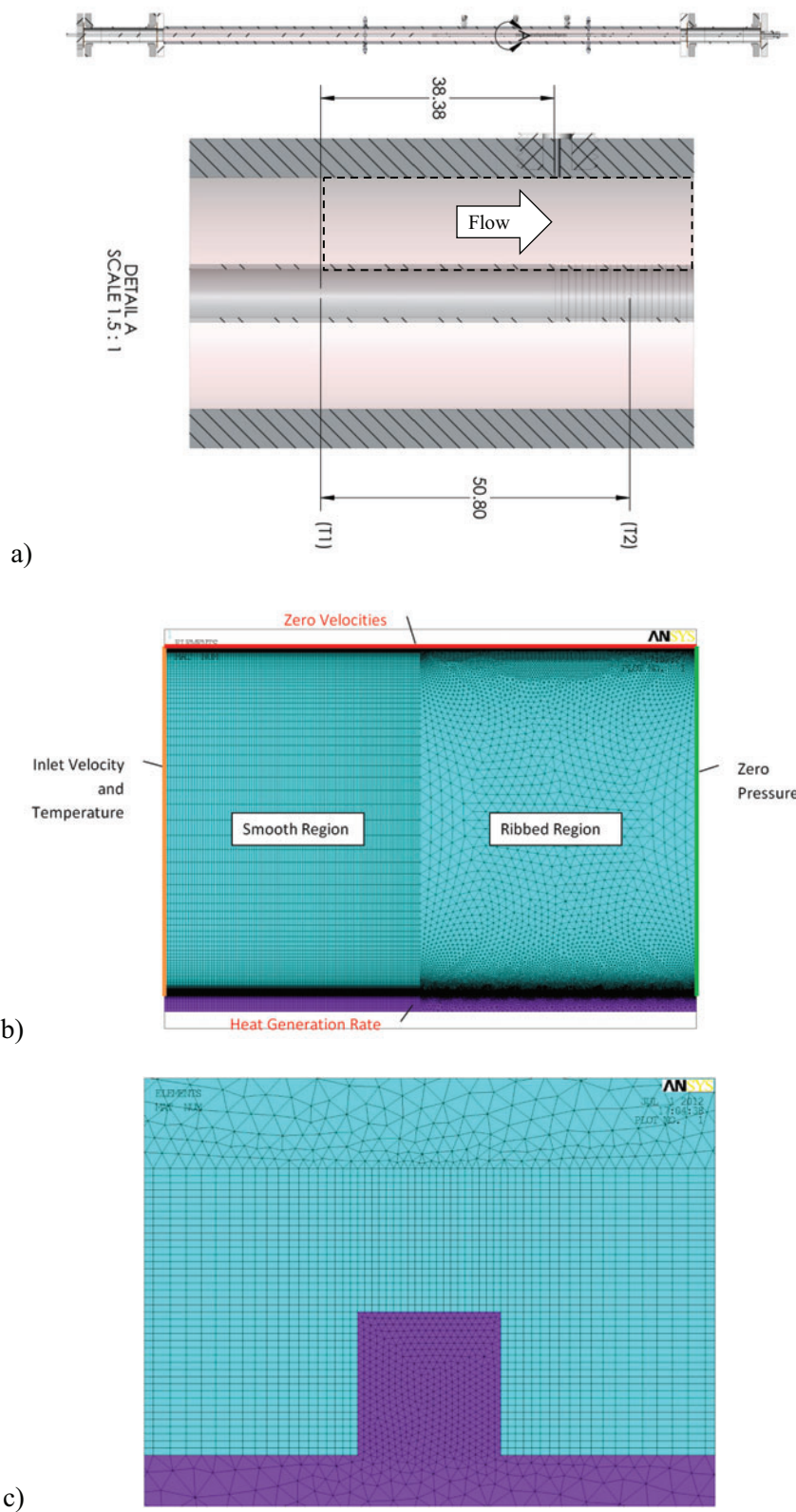
Figure 4. a) Axisymmetric CFD Flow Domain; b) CFD Model Boundary Conditions; c) Rib Mesh.

Table 3. Water and Inconel thermal properties

Material	Parameter	20°C	101.3°C	Unit
Water	density	1000	957	Kg/m^3
	viscosity	0.001	2.78x10^{-4}	Pa.s
	conductivity		0.68	W/m
	heat capacity		4217	J/(kg.°C)
			150°C	
Inconel	conductivity		11	W/m
	heat capacity		436	J/(kg.°C)
	density		8440	Kg/m^3

Table 4. CFD pressure drop and thermal analysis flow conditions

Analysis/Parameter	Pressure drop	Thermal	Unit
Inlet temperature	20	101.3	°C
Density	1000	957	Kg/m^3
Viscosity	0.001	2.78x10^{-4}	Pa.s
Conductivity	0.60	0.68	W/(m.°C)
Heat capacity	4184	4217	J/(kg.°C)
Reynolds number	10^5	117,000	
Inlet velocity	4.71	1.18	m/s

4. RESULTS AND DISCUSSIONS

4.1. Experimental Results

The lab team performed the cold flow pressure drop test at the beginning of the experimental program prior to the heat transfer tests. The tests were performed at eight different flow rates with ten readings of pressure difference at each flow rate. Fig. 5a shows the friction factor data as a function of Reynolds number associated with the smooth and the ribbed surfaces.

Fig. 5b shows that the experimental friction factor data obtained for the smooth rod agree reasonably well with those based on Haaland [16] equation for smooth surfaces. The experimental results indicate an increase in friction factor varying from 37 to 50% at Reynolds numbers ranging from 43,000 to 90,900 at 20°C. Therefore, the expression that best represent the flow resistance test data at the ribbed surface with 95% of confidence is

$$f_r = 7.557 \times 10^{-3} - 2.776 \times 10^{-9} \, \text{Re} \pm 2.66 \times 10^{-4}$$

The heat balance check followed the differential pressure tests. The loop was heated up to a steady state condition by supplying 3.2 kW to the heater rod at system pressure of 0.5 MPa, inlet temperature of 38°C, and flow rate of 0.23 m^3/h. The analysis determined the heat loss to be approximately 8% under steady state conditions, which less than the assumed allowable limit of 10%.
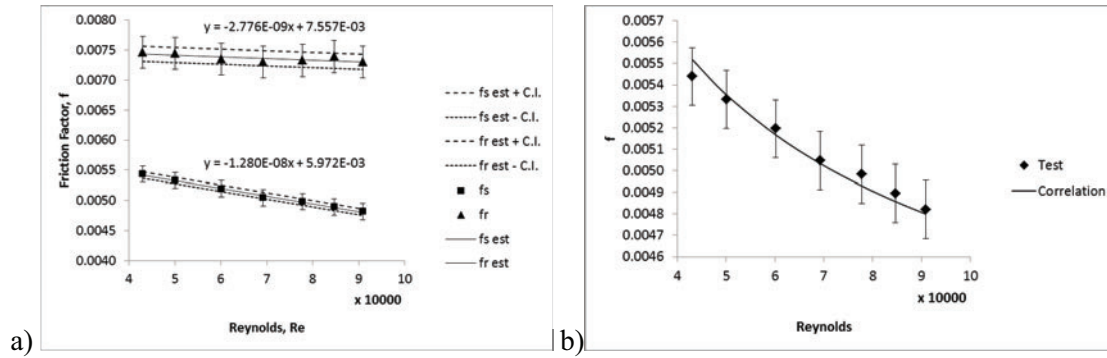
Figure 5. a) Friction Factor vs Reynolds Number at 20°C; b) Experimental Results compared to Haaland's Relation [16].
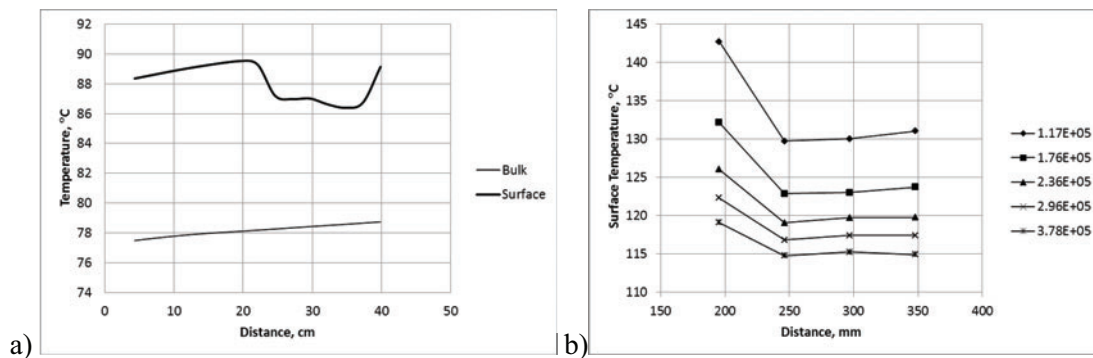
Figure 6. a) Bulk and Surface Temperature; b) Temperatures on Smooth and Ribbed Surfaces at various Reynolds Numbers.

Fig. 6a shows preliminary bulk and surface temperature profiles along the heated tube. These preliminary test data are important for selecting the minimum number of temperature acquisition points for the subsequent tests. In this case, the movable thermocouple measures the first temperature at 43 mm above the lower end of the heated tube. It also measures the next two temperatures in spans of 76.2 mm. In the roughened section, it measures eight points at every 25.4 mm elevation above the upper end of the smooth surface section. The measurements extend beyond the roughened section, when the tube surface is smooth again.

As expected, the differential temperature and, consequently, the heat transfer coefficient do not vary along the smooth surface. Therefore, the higher temperature point defined 195.4 mm above the lower end of the heated tube is sufficient to determine the smooth heat transfer coefficient. In the roughened section, the surface temperature is minimum at approximately 348 mm above the lower end of the heated tube. Therefore, the minimum temperature point, added of two more points, arranged in spans of 50.8 mm, are sufficient to describe the heat transfer coefficient profile along the roughened section. Fig. 6b shows the temperature profile between smooth and ribbed surfaces at various Reynolds numbers.

Fig. 7a shows the Nusselt with the Reynolds number correlation for smooth and ribbed surfaces. In both cases, the heat transfer data assume a linear behavior. A comparison between experimental results and Nusselt number calculated from Gnielinski's [17] equation shows good agreement (Fig. 7b).
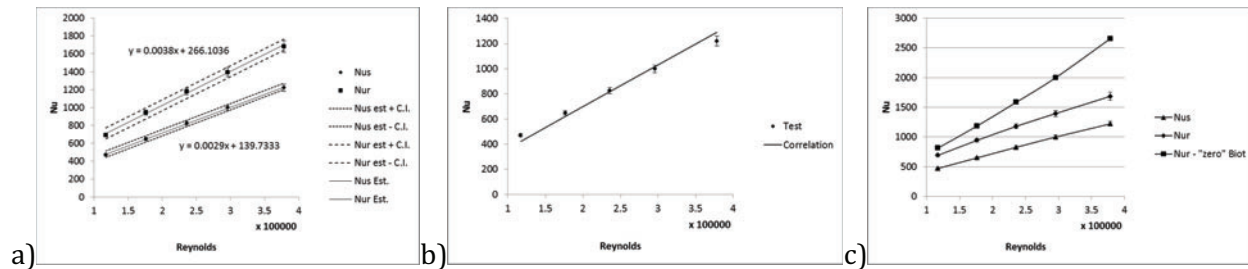
Figure 7. a) Heat Transfer vs Reynolds Numbers at 102°C; b) Experimental Results compared to Gnielinski's Relation; c) Experimental Results compared to Zero Biot Adjusted Data.

The test results indicate an increase in heat transfer varying from 47% to 38% at Reynolds numbers ranging from 117,000 to 378,000, and Prandtl number ranging from 1.69 to 1.71. Note that, the heat transfer enhancement decreases as the flow rate increases. The heat transfer results across the smooth and the ribbed surfaces are calculated from the experimental test data are represented by the following equations:

$$Nu_s = 139.73 + 0.0029\,\text{Re} \pm 35.24 \text{ W/m}^2 \cdot {}^\circ\text{C}$$

$$Nu_r = 266.10 + 0.0038\,\text{Re} \pm 61.40 \text{ W/m}^2 \cdot {}^\circ\text{C}$$

As mentioned above, the temperatures measured on the ribbed surface may need to be adjusted due to the irregularity of the surface as the thermal conduction equation does not account for the ribs effect. Firth and Meyer [12] determined the adjustment factor from experiments with flowing gas. According to the proposed method, the test data is adjusted to zero Biot number according to the following equation:

$$E_\infty = 1 - 0.79 Bi$$

where

$$Bi = h \times U_r / k_r$$

In order to adjust the experimental heat transfer coefficient on the ribbed surface, $U_{r,\infty}$ is defined, as follows:

$$U_{r,\infty} = U_r / E_\infty$$

Fig. 7c shows the "zero" Biot adjusted data compared to the experimental results. According to this method, the heat transfer enhancement varies from 73% to 117%. In this case, the heat transfer enhancement increases with the flow rate.

4.2. CFD Analysis Results

The turbulent flow and the pressure drop results across the smooth and the ribbed surfaces of the heater tube at test conditions are presented below. Fig. 8a shows the velocity profiles at smooth and ribbed surfaces at fully developed flow conditions.

Fig. 9a presents the flow path between ribs with recirculation and reattachment points. These characteristics are important to understand the mechanisms responsible for the enhanced heat transfer. While recirculation points hold the highest temperatures, the reattachment points hold the highest heat transfer rates.
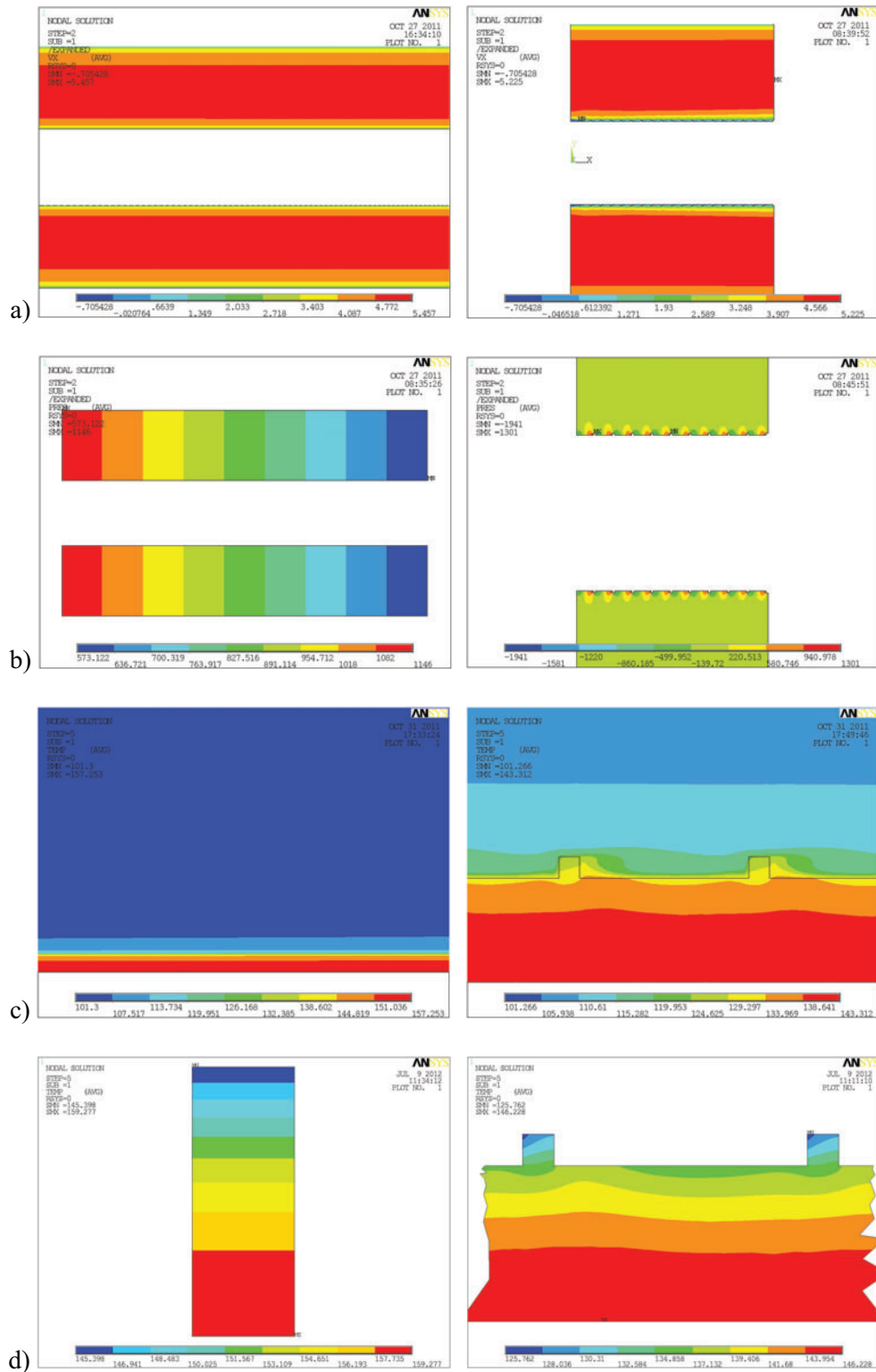
Figure 8. a) Velocities (m/s) in the smooth and ribbed sections; b) Differential pressure (Pa) on the smooth and ribbed surfaces; c) Smooth and ribbed walls and water temperatures (°C); d) Smooth and ribbed wall temperatures (°C).
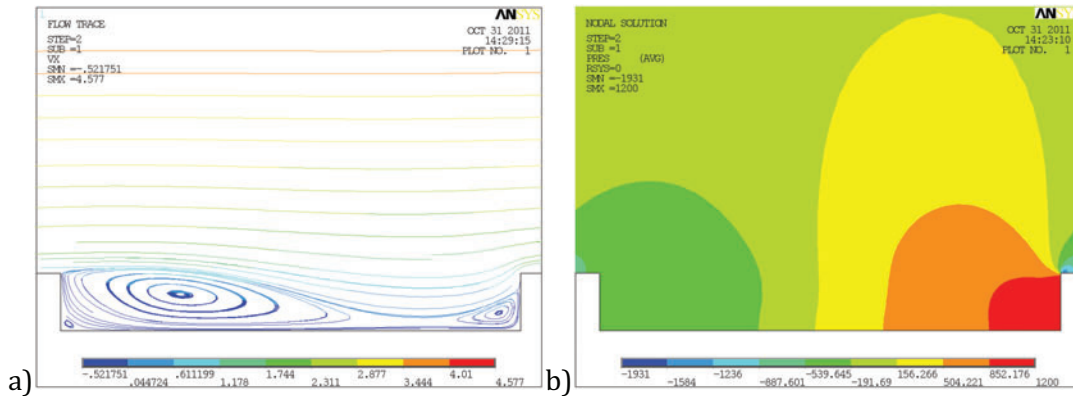
Figure 9. a) Flow path (m/s) between ribs; b) Differential pressure (Pa) between ribs.

Fig. 8b shows the differential pressure across the ribbed surface and Fig. 9b shows the results in more detail around the rib. As expected, the right-angle change due to the rib wall causes the flow to separate, resulting in negative pressures, and to reattach further downstream. The differential pressure result values are obtained from selected nodes and averaged over the smooth and the ribbed surfaces. Then, the friction factor is calculated using the following expression:

$$f = \Delta p \left(D_h / l \right) 2 \Big/ \rho V_{avg}^2$$

Fig. 8c shows the solid/fluid temperature distributions across the smooth and the ribbed surfaces of the heated tube model, respectively.

Fig. 8d shows the temperature distributions across the thickness of the heated tube wall at the smooth and the ribbed sections of the model.

The temperature results at the ribbed surface need a little more elaboration, as the geometry is irregular due to the ribs. In this case, the wall temperature results are averaged on the surface, along one pitch of ribs, as follows:

$$T_{w,avg} = \int_{pitch} T_w ldl \Big/ pitch$$

Next, the averaged values are added to the heat transfer rate equation, below, for calculation of the heat transfer for comparison with the test data.

$$U = q \Big/ A_s \left(T_w - T_b \right)$$

$$Nu = U D_h \Big/ k$$

Tables 5 and 6 compare the CFD and the experimental results for flow resistance and heat transfer, respectively. The numerical results of flow resistance and temperature are approx. 3% and 2% higher, respectively, when compared to the experiment.

The CFD model also shows a slight temperature variation along the simulated fuel rod. This indicates that, the thermal conduction effect on heat transfer is negligible. This is expected as the heated Inconel tube has a very thin wall, 0.75 mm.

Table 5. Friction factor, CFD vs experimental results at 20°C and Re = 100,000

Surface	CFD	Test	Ratio
Smooth	4.97×10^{-3}	4.82×10^{-3}	1.03
Ribbed	7.45×10^{-3}	7.30×10^{-3}	1.02
Increase	1.50	1.51	

Table 6. Heat transfer, CFD vs experimental results at 101.3°C and Re = 117,000

Parameter	Surface	CFD	Test	Ratio
Temperature (°C)	Smooth ID	159.3	158.9	1.003
	Smooth OD	145.4	142.7	1.019
	Ribbed ID	146.2	145.9	1.002
	Ribbed OD	130.9*	129.8	1.008
Heat Transfer (Nusselt)	Smooth OD	442	471	0.938
	Ribbed OD	665	691	0.962
Enhancement		1.50	1.47	1.020

Some solution strategies showed to be very effective to facilitate convergence of the results, they are: initializing the flow solution with temperature solution deactivated; setting the relaxation factor for temperature to one for constant fluid properties; initializing the temperature field in the solution domain at one iteration. This conjugate heat transfer CFD model requires a significant number of iterations for convergence of the temperature results. It requires 5,000 iterations for the flow and other 20,000 iterations for the temperature solution. The convergence criterion is based on the difference between solutions in terms of velocity results. A difference of approximately 1% is acceptable. The mesh size independence of the results relies on the y^+ criterion as previously mentioned.

5. CONCLUSIONS AND RECOMMENDATIONS

This study tested the heat transfer and friction factor correlations based on Firth and Meyer [12], Ravigururajan and Bergles [13], and Meyer [15] work, at typical PWR conditions. These correlations suggest that a roughened rod surface with transverse square ribs can improve heat transfer in PWR rod bundles by at least a factor of 1.73. However, the experimental and the numerical results obtained by this research show strong evidence that transverse square ribs can improve heat transfer in PWR rod bundles by a factor of approximately 1.50. Therefore, those correlations seem to over predict the heat transfer enhancement at PWR conditions. Table 7 presents a comparison between the heat transfer enhancement ratios obtained at Re=117,000 and water temperature of 101.3°C.

The present work indicates that, in order to deliver 50% heat transfer enhancement, the transverse square rib shape shall present parameters of height and width of 0.127 mm, and pitch of ribs equals to 9 times the height for a rod diameter of 9.5 mm.

Regarding the numerical study, the CFD model results are 3% higher for differential pressure and 2% higher for temperature, when compared to the experiment (Tables 5 and 6). Considering typical test data uncertainties, the agreement between the test and the numerical results is satisfactory. Therefore, the CFD model developed for this analysis is suitable to calculate differential pressure and convective single-phase heat transfer at smooth and square ribbed surfaces in turbulent flows.

Table 7. Heat transfer enhancement ratios by different methods

Method	Nu_r/Nu_s
This Experiment	1.47
This CFD	1.50
Firth and Meyer	1.73
Ravigururajan and Bergles	2.50
Meyer	2.40

The friction factor results show a maximum increase in flow resistance of approximately 50%. In order to estimate the heat transfer enhancement and the increase in pressure drop in real rod bundles, the test data obtained by this research needs to be converted from annular to rod bundle boundary conditions. This transformation can be done analytically, based on empirical correlations, or numerically by modeling at least two rod bundle sub channels [21]. However, it is always recommended to perform an experimental test to confirm the analysis results.

Although the artificial roughness increases the friction losses on the rods, this may be fully or partially compensated by removing the mixing vanes and the associated pressure drop on the top of the fuel assembly spacer grids. Hence, the global turbulence due to the mixing vanes would be substituted by a local and uniform turbulence generated by the artificial roughness design.

Another suggestion is to implement the roughened surface only in the upper region of the fuel rod where the temperatures are higher, as such reducing friction losses. Also, a rod vibration test should be performed to evaluate the local turbulence effects and its impact on the fretting wear margin.

Another concern is the probability of a substantial increase in crud deposition on the ribbed surface during PWR operating conditions. A few basic improvements can be done in order to mitigate it, though. For example, the ribbed roughness could be redesigned from transverse to a helical configuration. This design would allow the water to flow between the ribs, as such minimizing stagnation that could contribute for the crud to deposit. In addition, the rib could be redesigned from square to a curved shape profile. This design would not only reduce crud hang-up points due to the sharp corners of a square shape, but also reduce peaking temperatures caused by recirculation points between ribs and the base surface. Note that, the latter should not be a concern as the maximum temperature predicted by CFD in the ribbed section wall is slightly higher than the minimum temperature in the smooth section wall.

Finally, it is expected that the proposed roughness design can generate uniform heat transfer along the PWR fuel rods, minimizing peaking temperatures and its undesirable consequences.

NOMENCLATURE

A	Cross Sectional Area		Pr	Prandtl Number
Af	Flow Area		P_w	Wet Perimeter
A_s	Surface Area		q	Power Rate
Bi	Biot Number		$\dot{q}$	Heat Generation Rate per Unit Volume
d_{eq}	Equivalent Inner Diameter		Q	Water Flow Rate
d_o	Tube Outer Diameter		R	Electrical Resistance
d_i	Tube Inner Diameter		Re	Reynolds Number
D_h	Hydraulic Diameter		T	Temperature
E	Electrical Voltage		T_b	Bulk Temperature
f	Friction Factor		T_w	Surface Temperature
f_r	Friction Factor on the Ribbed Surface		$T_{w,i}$	Inner Surface Temperature
f_s	Friction Factor on the Smooth Surface		U	Heat Transfer Coefficient
h	Rib Height		U_s	H. Transfer Coef. at the Smooth Surface
H	Enthalpy		U_r	H. Transfer Coef. at the Ribbed Surface
I	Electrical Current		V	Velocity
k	Thermal Conductivity		V_{avg}	Average Velocity
k_r	Thermal Cond. in the Ribbed Section		w	Rib Width
k_s	Roughness Height		W	Square Flow Housing Width
l	Length			
$\dot{m}$	Mass Flow Rate		Δ_p	Differential Pressure
Nu	Nusselt Number		μ	Fluid Viscosity
Nu_r	Nusselt Number on the Ribbed Surface		ρ	Fluid Density
Nu_s	Nusselt Number on the Smooth Surface		ρ_e	Electrical Resistivity
p	Pitch of Ribs		τ_w	Wall Shear Stress
p_r	Pitch of Rods			

REFERENCES

1. K. Rehme and G. Trippe, "Pressure Drop and Velocity Distribution in Rod Bundles with Spacer Grids," *Nucl. Eng. Design*, **62**, pp. 349-359 (1980).
2. Z. Karoutas et al, "3-D Flow Analyses for Design of Nuclear Fuel Spacer," *Proceedings of the 7th Int. Meeting on Nuclear Reactor Thermal-Hydraulics NURETH-7*, **1**, pp. 3153-3174 (1995).
3. J. Nikuradse, "Laws of Flow in Rough Pipes," NACA, TM 1292, Washington (1950). Translation of "Strömungsgesetze in rauhen Rohren," VDI-Forschungsheft 361. Beilage zu "Forschung auf dem Gebiete des Ingenieurwesens," Ausgabe B Band 4, July-August (1933).
4. D. F. Dippery and R. H. Sabersky, "Heat and Momentum Transfer in Smooth and Rough Tubes at Various Prandtl Numbers," *Int. J. Heat Mass Transfer*, **6**, pp. 329-353 (1963).
5. L. S. Tong et al, "DNB on a Finned Surface Heater Rod," *Westinghouse Commercial Atomic Power Topical Report WCAP-2944*, Westinghouse Proprietary, June (1966).
6. M. D. Donne and L. Meyer, "Turbulent convective heat transfer from rough surfaces with two-dimensional rectangular ribs," *Int. J. Heat and Mass Transfer*, **20**, 583-620 (1977).

7. L. D. Gee and R. L. Webb, "Forced Convection Heat Transfer in Helically Rib-Roughened Tubes," *Int. J. Heat Mass Transfer*, **23**, pp. 1127-1136 (1980).

8. L. Meyer, "Heat Transfer and Pressure Drop at Single Rods with Three-Dimensional Roughnesses: Large Scale Tests," *Institut für Neutronenphysik und Reaktortechnik KfK 3164*, Kernforschungszentrum Karlsruhe, Karlsruhe , April (1981).

9. L. Meyer and W. Neu, "Heat Transfer and Pressure Drop at Single Pins with Three-dimensional Roughnesses," *Institut für Neutronenphysik und Reaktortechnik KfK 3165*, Kernforschungszentrum Karlsruhe, Karlsruhe , April (1981).

10. L. Meyer, "Thermohydraulic Characteristics of Single Rods with Three-Dimensional Roughness," *Int. J. Heat Mass Transfer*, **25** (7), pp. 1043-1058 (1982).

11. R. J. Firth, "An interpretation of the KfK heat transfer data for three-dimensional roughness, Gas Cooled Reactors Today," *BNES*, pp. 205-210, London (1982).

12. R. J. Firth and L. Meyer, "A Comparison of the Heat Transfer and Friction Factor Performance of Four Different Types of Artificially Roughened Surface," *Int. J. Heat Mass Transfer*, **26** (2), pp. 175-183 (1983).

13. T. S. Ravigururajan and A. E. Bergles, "Development and Verification of General Correlations for Pressure Drop and Heat Transfer in Single-Phase Turbulent Flow in Enhanced Tubes," *Experimental Thermal and Fluid Science*, **13**, pp. 55-70 (1996).

14. P. Dimitrakopoulos and J. J. L. Higdon, "On the displacement of three-dimensional fluid droplets from solid surfaces in low-Reynolds-numbers shear flows," *J. Fluid Mech.*, **377**, pp. 189-222 (1998).

15. L. Meyer et al, "Enhancement of Heat Transfer in Fuel Assemblies of High Performance Light Water Reactors," *J. Nucl. Sci. Tech.*, **44** (3), pp. 270-276 (2007).

16. S. E. Haaland, "Simple and Explicity Formulas for the Friction Factor in Turbulent Pipe Flow," *J. Fluids Engineering*, **105**, pp. 89-90 (1983).

17. V. Gnielinski, "New equations for heat and mass transfer in turbulent pipe and channel flow," *Int. Chem. Eng.*, **16** (2), pp. 359-367 (1976).

18. L. A. Carrilho et al, "Two and three-dimensional simulations of enhanced heat transfer in nuclear fuel rod bundles," *ASME Summer Heat Transfer Conference*, San Francisco (2009).

19. D. C. Wilcox, "Reassessment of the Scale-Determining Equation for Advanced Turbulence Models," *AIAA Journal*, **26**, pp. 1299-1310 (1988).

20. F. R. Menter, "Two-Equation Eddy-Viscosity Turbulence Models for Engineering Applications," AIAA Journal, **32**, pp. 1598–1605 (1994).

21. L. A. Carrilho and J. A. Khan, "Modeling of the effect of parallel rib-type roughness on local, single-phase heat transfer in rod bundles by CFD – Part 1: Flow Resistance," *18th Int. Conf. Nuclear Eng. ICONE-18*, Xi'an, China (2010).